Molecular Crystals and Liquid Crystals
Publication details, including instructions for authors and subscription information:
http://www.tandfonline.com/loi/gmcl16

X-Ray Study Of Freely Suspended Films Of A Multilamellar Lipid System

G. S. Smith [c a], C. R. Safinya [a], D. Roux [b a] & N. A. Clark [c a]

[a] Exxon Research and Engineering Co., Annandale, NJ, 08801

[b] CRPP and Greco microemulsion, 33405, Talence, France

[c] University of Colorado, Boulder, CO, 80309

Version of record first published: 21 Mar 2007.

To cite this article: G. S. Smith , C. R. Safinya , D. Roux & N. A. Clark (1987): X-Ray Study Of Freely Suspended Films Of A Multilamellar Lipid System, Molecular Crystals and Liquid Crystals, 144:5, 235-255

To link to this article: http://dx.doi.org/10.1080/15421408708084218

Mol. Cryst. Liq. Cryst., 1987, Vol. 144, pp. 235–255
Photocopying permitted by license only

Printed in the United States of America

X-Ray Study Of Freely Suspended Films Of A Multilamellar Lipid System

G. S. SMITH[a,c], C. R. SAFINYA[a], D. ROUX[a,b] and N. A. CLARK[c]

[a] *Exxon Research and Engineering Co., Annandale, NJ 08801*
[b] *CRPP and Greco microemulsion, 33405 Talence, France*
[c] *University of Colorado, Boulder, CO 80309*

(*Received August 20, 1986*)

We report the first x-ray scattering measurements from freely suspended lipid(DMPC)-water multilayer films. By combining several techniques, we are able to grow stable, oriented films of various thicknesses ($\sim 10^2$ to 10^4 Å) in a controlled temperature (0°C to 80°C) and humidity (0% to 100%) environment. A specially designed film holder allows both transmission and reflection x-ray measurements. Very importantly, the humidity control system allows us to construct the temperature-chemical potential phase diagram in addition to the normally studied temperature-concentration phase diagram. Our most important results are as follows. First, we find a metastable L_α phase in bulk DMPC-water mixtures when the water concentration is between 30 and 40 weight percent, and second, from the variation of the interplanar peak position as a function of concentration and chemical potential, we are able to deduce the functional form of the interaction force between layers in the L_α phase. This form is found to be consistent with a repulsive short range hydration force. Independently, x-ray reflectivity measurements of eight harmonics of the structure factor in the L_α phase are consistent with the existence of strong short range interactions between the layers.

Keywords: phospholipid, membrane, x-ray diffraction, hydration force, phase diagram, chemical potential, film

I. INTRODUCTION

Phospholipids are amphiphilic molecules known to form the basis for biological cell membranes. When these molecules are mixed with water they form a multitude of interesting phases.[1] It is thought that the formation of particular phases in the cell membrane plays a role in certain biological processes.[2] Therefore, the study of the structure

and the physical properties of these phases is of fundamental interest in biology. Particularly, an understanding of the interactions between cells may be gained through the study of multilamellar lipid membranes.

When phospholipid molecules are mixed with a small amount of water, they stack in a system of multilayers forming smectic liquid crystals. These amphiphilic molecules organize in bilayers separated by water such that the head groups lie at the lipid-water interface. As the concentration of water increases, the distance between the bilayers increases. When the distance between layers reaches a limiting value, d_l, the excess water phase-separates from the liquid crystal indicating a minimum in the interaction energy as a function of the d-spacing. This minimum comes from the competition between long range van der Waals attraction and short range repulsive forces. The latter have been identified as exponential electrostatic and hydration forces.[3,4]

In addition to these basic forces, Helfrich[5] has proposed a novel type of mechanism which leads to a long range repulsive interaction which under suitable conditions competes with the van der Waals interaction. This interaction results from thermally induced out-of-plane layer fluctuations stericly hindered in a multilayer system. More generally, steric repulsion is known to be the dominant interaction associated with wandering walls of incommensurate phases.[19] Recent high resolution x-ray work has in fact shown that steric interactions dominate in the multilamellar L_α phase of the quaternary mixture of sodium dodecyl sulfate, water, dodecane, and pentanol.[6] The relevance of this interaction in biological multilayer systems, however, is unclear and largely controversial.

Aside from intermembrane interaction forces, structural information regarding biomembranes may be gathered by studying phospholipid-water mixtures. Indeed, these materials exhibit a large variety of liquid-crystal and crystal phases. Three of the lamellar phases are especially relevant to biological systems.[1] At high temperatures, the phospholipid molecules are liquid-like without intermolecular order. As a function of decreasing temperature, there is a first order phase transition to different phases (depending on the water content of the lipid-water system) where the hydrocarbon chains are frozen in various ordered configurations. One of these phases consists of flat bilayers with the frozen hydrocarbon chains either tilted ($L_{\beta'}$) or not (L_β).[1,7] The other low temperature phase, the $P_{\beta'}$ (or P_β) phase is thought to be similar to the $L_{\beta'}$ (or L_β) phase with the addition of a long-wavelength in-plane modulation.[7] The exact structure of this phase is not understood and in fact, the nature of the L_α-$P_{\beta'}$ and $L_{\beta'}$-

$P_{\beta'}$ phase transitions with the onset of the modulation constitutes one of the most glaringly unresolved problems in this field.

After years of intensive work, many of the important questions about the structure of these phases and about the interactions between bilayers remain unanswered. This is mainly due to the fact that it is difficult to prepare large, well aligned crystals of this material. To date, most experiments have been performed on unoriented samples in the presence of excess water. The structure of the phases, particularly the $P_{\beta'}$ phase, is difficult to resolve in such polycrystalline samples.

A very powerful and successful technique used to produce large single crystal domains of thermotropic liquid crystals is the method of the freely suspended film. Used to study a smectic material, this technique produces a film where the planes are oriented parallel to the liquid crystal-air interface.[8,9,10] The thickness of the film can vary depending on the amount of material used and on the speed with which the film is drawn. It was suggested by Pershan[21] that under controlled humidity this same technique may be used for lyotropic liquid crystals.

In this paper, we report the first results obtained using the freely suspended film technique to study a multilamellar system of phospholipids plus water. These films are only stable under controlled vapor pressure conditions. Therefore, we have designed and built a humidity system capable of controlling the relative humidity from 0% to 100% over a temperature range of 0°C to 80°C. The details of this system and our film oven are presented in Part II. Also in Part II, we present a new film holder design. In the past, x-ray studies of freely suspended films[8,9,10] were restricted to the transmission geometry. Very importantly, in addition to transmission geometry, we are able to carry out x-ray reflection studies which allow us for example to access the $(0,0,\ell)$ Bragg reflections (that is the structure factor associated with the layering) in the L_α phase. In addition in the reflection geometry, by studying the Fresnel reflectivity from the surface of the film, one should in principle be able to extract information about the surface structure (for example surface roughness) of films under tension. The technique for such x-ray reflection studies was first pioneered by Als-Nielsen, Christensen, and Pershan[20] in connection with measurements done at a free air-liquid crystal interface.

With data obtained using our new oven, we have mapped the temperature-chemical potential (T-μ) phase diagram. By combining this information with the temperature-concentration (T-C) phase diagram, we find a region of metastability in the phase diagram of bulk

samples of DMPC-water mixtures with water content between 30 and 40 weight percent. Additionally, the (T-μ) and (T-C) phase diagrams indicate that the intermembrane forces are dominated by strong short range hydration forces. This is presented in detail in Part III. Independently, we have carried out x-ray measurements of the first eight harmonics of the interplanar structure factor in the L_α phase of a thick (>1 micron) freely suspended film. This data, presented in Part IV, also reveals that the interplanar forces are relatively strong in this system. Finally, we conclude with a summary of our results and a discussion of future experiments.

II. EXPERIMENTAL DETAILS

The main problem in dealing with a multicomponent system when at least one of the constituents is volatile is to control the relative amount of each substance. In the simplest case where the only volatile component is water, this can be achieved by controlling the humidity of the sample environment. We have chosen to build a film oven specifically designed for X-ray scattering experiments where the temperature and the humidity of the gas phase are controlled (Figure 1). Also, the temperature of the sample is separately controlled using thermoelectric devices. The relative humidity of the gas (nitrogen in our case) is regulated using a method similar to that of Gruner.[11] Figure 2 shows a schematic representation of our system. The humidity is adjusted to a suitable value by mixing dry and water saturated nitrogen in controlled proportions. When dewpoints in excess of room temperature are required, the entire system including the lines to and from the oven is heated to prevent condensation of the water vapor. The measurement of the humidity is made using dewpoint hygrometers on both the input and output sides of the reservoir (Figure 2) to check for equilibrium in the binary mixture. This information is relayed to a computer controlled system which opens and closes solenoid valves S1-S4 (Figure 2) in order to maintain the preset dewpoint.

To perform both transmission and reflection x-ray scattering experiments, the circular film hole[10] is replaced with a rectangular hole. Figure 3 shows the sample holder used to access the two geometries. Such an elongated shape is needed to assure that the beam hits only the film even at very small incident angles of about a degree.

The sample is prepared as follows. We make an arbitrary mixture of pure DMPC (>99%, Avanti Polar Lipids, Birmingham, Alabama) and distilled water. This mixture is then smeared around the edge of

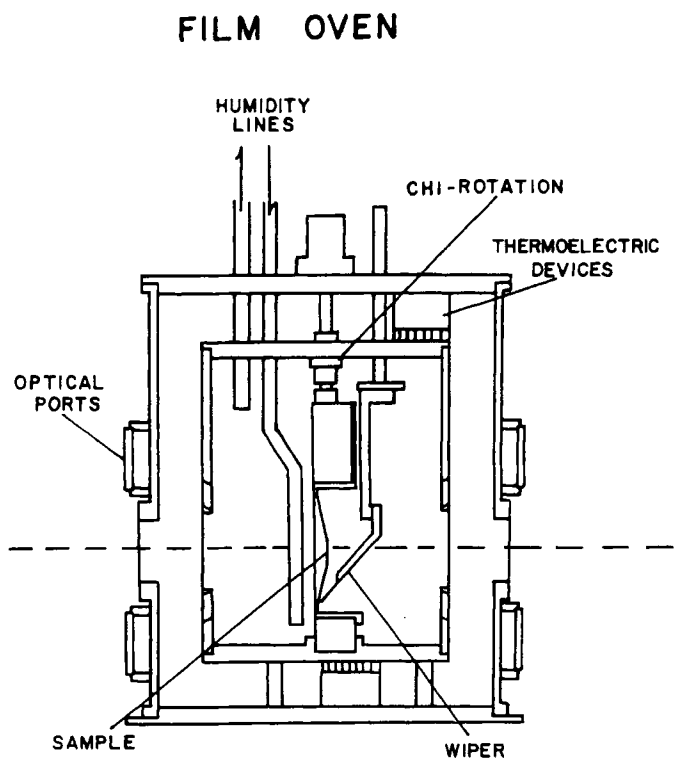

FIGURE 1 Schematic diagram of the x-ray film oven.

the hole in the film holder. The wiper assembly is quickly sealed in the oven, and the temperature and the relative humidity (R.H.) are fixed at values high enough to assure that the sample remains in the L_α phase (T~40°C and R.H.~100%). The film is drawn after a few minutes. The thickness of the film depends on the mixture prepared, the temperature, and the speed at which it is drawn. Once the film is drawn, the equilibrium state is reached after several minutes. After the initial or any subsequent change in temperature or humidity, X-ray measurements are repeated until the new equilibrium state is reached.

The oven and its temperature-humidity controlled system are used to perform X-ray studies. Three different spectrometer configurations are employed each having a different resolution function. A low resolution (LR) set up is used in house with an 18 kw rotating anode machine (Rigaku-RU300). The monochromator consists of a focusing bent pyrolitic graphite (002) crystal. Horizontal and vertical slits are positioned before and after the sample to define the in-plane and

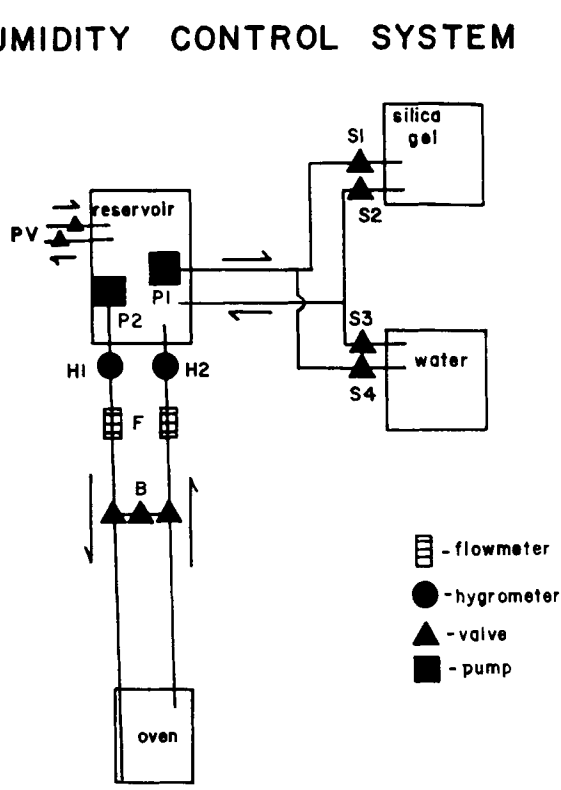

FIGURE 2 Schematic representation of the humidity control system.

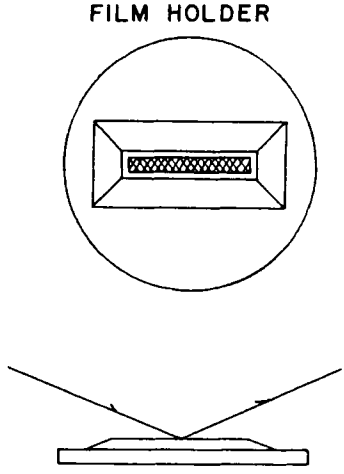

FIGURE 3 Schematic diagram of the film holder. The cross hatched area represents the film position.

out-of-plane resolutions. A high resolution (HR) spectrometer is also set up in house where the monochromator is a flat Ge (111) crystal. In this case, the analyzer is also a flat Ge (111) crystal in order to have comparable resolution before and after the sample. In addition, a very high resolution (VHR) set-up at the Exxon beam line X10A at the National Synchrotron Light Source (NSLS) at Brookhaven National Laboratory is employed. It consists of a double bounce Si(111) monochromator and a triple bounce Si(111) crystal as analyzer. Table I gives the different longitudinal resolution widths quoted as the half width at half maximum (HWHM) for each set-up.

III. PHASE DIAGRAMS

The phase diagram of a multicomponent system is usually represented as a function of mixed variables: a) fields (such as temperature or pressure) and b) densities (concentrations). To describe a binary mixture one needs three variables. In most cases, however, for fixed atmospheric pressure, the phase diagram may be described with only two variables. For the experimentalist, the most accessible variables are the temperature (field) and the concentration (density). The immediate consequence of such a representation is the existence of polyphase regions which are represented as surfaces separating the different one-phase regions. A more powerful but experimentally difficult representation of the phase diagram is the temperature versus chemical potential (μ, which is a field) phase diagram. In this representation, a region of two-phase equilibrium is simply depicted by a line since the chemical potential is the same for two phases in equilibrium. Moreover, the knowledge of the chemical potential as

TABLE I

Spectrometer configurations and their longitudinal resolutions.

Spectrometer Configuration	X-Ray Source	Monochromator, Analyzer	Longitudinal Resolution (HWHM)
Low Resolution (LR)	18kw rotating anode	focusing graphite, .5mm slits	.005Å^{-1}
High Resolution (HR)	18kw rotating anode	Ge(111), Ge(111)	.00028 Å^{-1}
Very High Resolution (VHR)	beamline X10A at NSLS	double bounce Si(111),triple bounce Si(111)	.00009Å^{-1}

a function of the concentration allows direct access to thermodynamic quantities. For example, knowing the chemical potential as a function of the intermembrane spacing in a lamellar phase allows one to calculate the interactions between the layers.[4]

Since we are able to control both the temperature and the chemical potential, we can access the entire phase diagram, and by using X-rays we can characterize the various phases. However, in order to compare our results with those of others and to have information on the *T-C* phase diagram, we have remapped the part of the *T-C* phase diagram in the vicinity of the L_α-$P_{\beta'}$-$L_{\beta'}$ triple point. We will first discuss the *T-C* phase diagram then the *T*-μ representation. Finally, we will compare the two phase diagrams and calculate the interaction forces between the layers in the L_α phase.

Temperature-concentration phase diagram

The temperature versus concentration phase diagram was determined as follows. Samples were prepared by mixing known quantities of DMPC and water. The concentration is calculated from the weight of each component. A predetermined mixture is then placed in a capillary and sealed. This procedure produces randomly oriented domains although the domain sizes (L) are unusually large ($L \geqslant 1$ micron). The capillary is placed in an oven and the X-ray diffraction patterns are measured at several temperatures. As a function of temperature, the L_α, $P_{\beta'}$, and $L_{\beta'}$ phases have been studied using the LR and HR spectrometers. These phases are easily characterized since the X-ray pattern of each is very different. Figure 4 shows typical longitudinal scans in reciprocal space in each of these three different phases.

From the position of the first order $(0,0,\ell)$ peak, we are able to deduce the d-spacing. Figure 5 gives the evolution of the first order peak position $q_0 (= 2\pi/d$ where d is the interplanar repeat spacing) as a function of temperature for different water concentrations. Starting in the L_α phase, the position of the first order peak decreases with temperature. A sudden decrease in the value of q_0 characterizes the phase transition to the $P_{\beta'}$ phase, and at the same time, a peak at $q = 0.04$-0.05 Å^{-1} appears (Figure 4b). At still lower temperatures, another jump to a higher value of q_0 corresponds to the transition into the $L_{\beta'}$ phase which has no peak at small q-vector (Figure 4c). We note that the ordered $L_{\beta'}$ phase is readily distinguished from the L_α phase by the appearance of a sharp high angle peak at $q \cong 1.4$Å^{-1} in the $L_{\beta'}$ phase associated with long range positional order of the

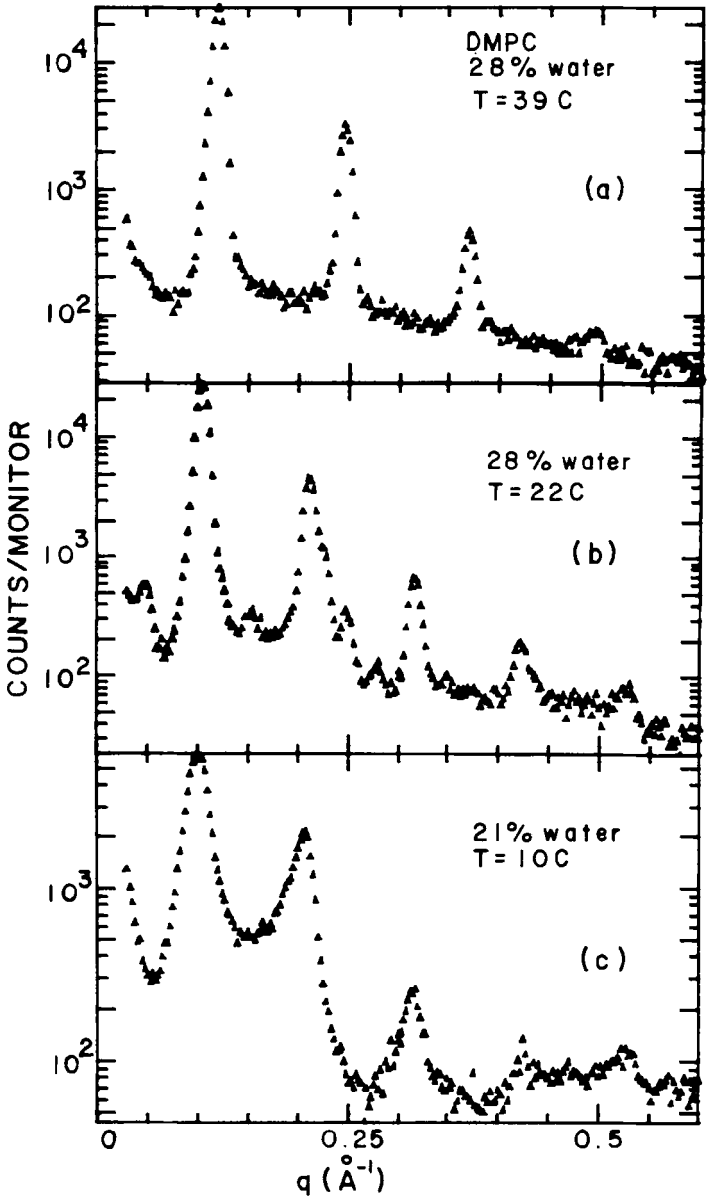

FIGURE 4 Longitudinal scans in reciprocal space plotted on a logarithmic intensity scale of DMPC-water mixtures in the (a)L_α, (b)$P_{\beta'}$, and the (c)$L_{\beta'}$ phases. Note the appearance of the modulation peak in the $P_{\beta'}$ phase at $q \sim 0.05$ Å^{-1}.

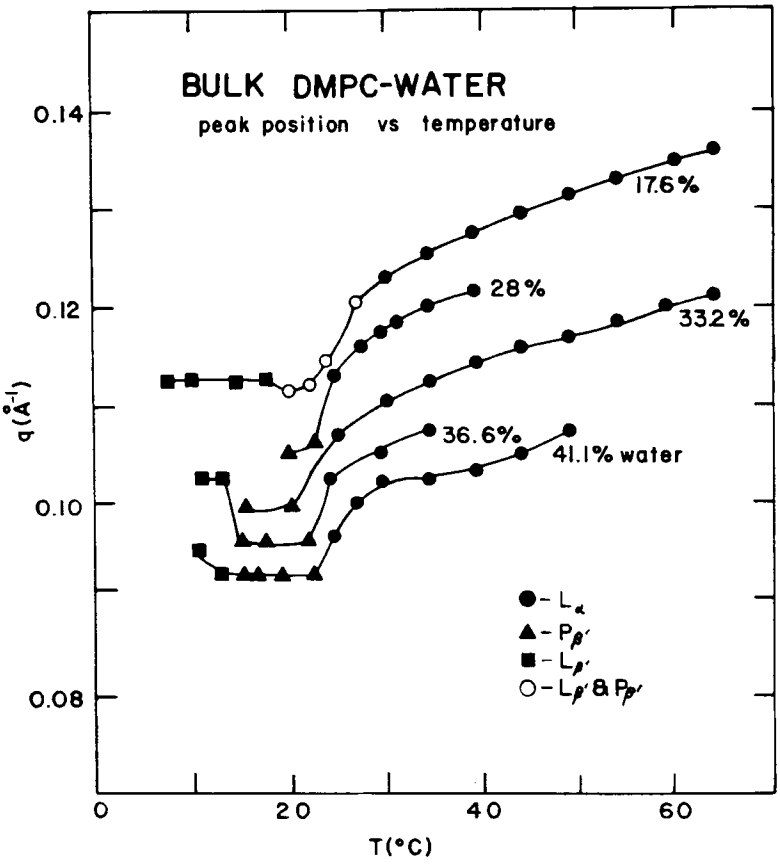

FIGURE 5 The peak position of the first harmonic as a function of temperature and concentration.

molecules in each layer (Figure 7c). In the disordered L_α phase, the high angle peak centered at $q \cong 1.4 Å^{-1}$ is broad which is indicative of liquid-like order of the molecules in the layers (Figure 7a). From these measurements, the *T-C* phase diagram can be drawn (Figure 6). This phase diagram is in agreement with those published previously.[7,1] It is important to note that the maximum *d*-spacing in the three phases corresponds to a water content of ~40 weight percent. For water concentrations larger than this limiting value, the *d*-spacing is constant. This indicates a phase-separation between the liquid crystal phase and pure water.

Temperature versus chemical potential phase diagram

Using the set-up described in Part II, we are able to perform phase diagram determinations on a film while controlling the vapor pressure instead of the concentration. Since the water vapor can be considered a perfect gas, the difference between the chemical potential of pure water and the chemical potential of the binary mixture is given by:

$$(\mu - \mu_0) = \Delta\mu = RT \,\mathrm{Log}(P/P_0) \qquad (1)$$

where P is the vapor presusre of the binary mixture at the temperature T and P_0 is the vapor pressure of the puree water at the same temperature. The relative humidity, P/P_0, is fixed experimentally and the d-spacing is measured with X-rays in two ways. The first method consists of drawing a film thick enough to avoid complete alignment of the domains. Using a sample prepared in this manner, the first order peak corresponding to the out-of-plane periodicity can be seen regardless of the sample orientation. This is very similar to our bulk

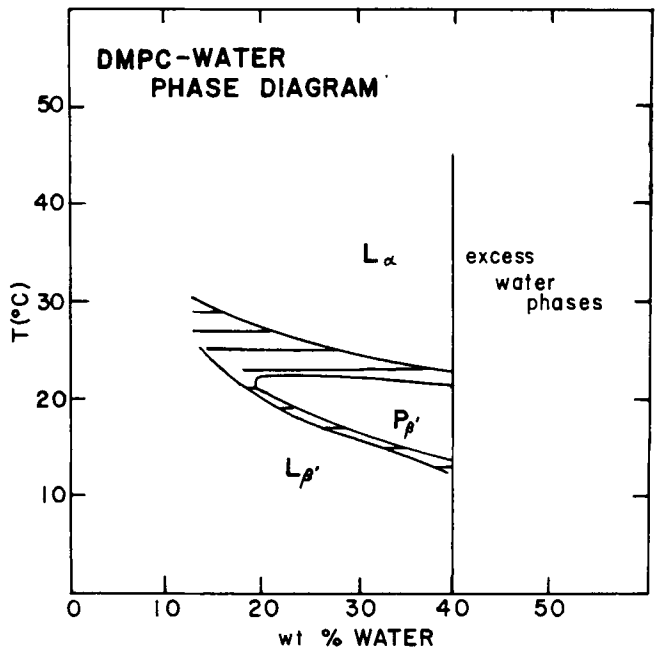

FIGURE 6 The temperature-concentration phase diagram for the DMPC-water binary system.

measurements; the only difference is that we control the chemical potential instead of the concentration. The second way was to measure the *d*-spacing of an oriented film in the reflection geometry. The advantage of the first method for mapping the phase diagram is indeed clear. This method is quick since there is no need to locate a single spot in three dimensional reciprocal space. In addition when the first method is used, we believe that the surface effects are negligible since the films are very thick and represent the bulk. Consequently, for mapping the phase diagram, we have primarily used the thick film method rather than the reflectivity method.

After drawing a thick film, the temperature is maintained at a constant value and x-ray measurements are performed over a range of humidities. Figure 7 shows a typical set of x-ray scans. We have checked that this method is reproducible by repeating several scans at a given relative humidity (either approached from above or below) using the same film. In all of the cases after several minutes, the *d*-spacing stabilizes at a reproducible value. With this data, the phase transition is located as a function of humidity. The resulting phase diagram is schematically represented in Figure 8.

Comparison of the phase diagrams

The two phase diagrams (Figures 6 and 8) agree qualtiatively but a quantitative comparison yeilds a striking difference. The phase transition with pure water is located at ~40% water concentration in the *T-C* phase diagram; however, the same transition which corresponds to 100% humidity is located at the equivalent of ~30% concentration in the *T*-μ phase diagram. In other words, the limiting *d*-spacing for lipids mixed with excess water is found to be 60 Å at 40°C, yet only 54 Å when the binary mixture is in equilibrium with the water saturated nitrogen (100% humidity). In order to check that the measurements have been performed at equilibrium, we can introduce into the oven a mixture of lipid with more than 40% water. By quickly drawing a film in an atmosphere of 100% humidity, we are able to see the *d*-spacing changing from 60 Å to 54 Å and stabilize at this latter value. To check that this difference was not only on the *d*-spacing but also on the limiting concentration, we put some dry lipids of known weight in a water saturated atmosphere for several days. Upon weighing the sample, we found that the limiting value of the adsorbed water was ~ 30% corresponding effectively to the value of 54 Å (at 40°C). In the literature, this phenomenon has been previously noted.[12] All of the experiments made with lipids in equilibrium with

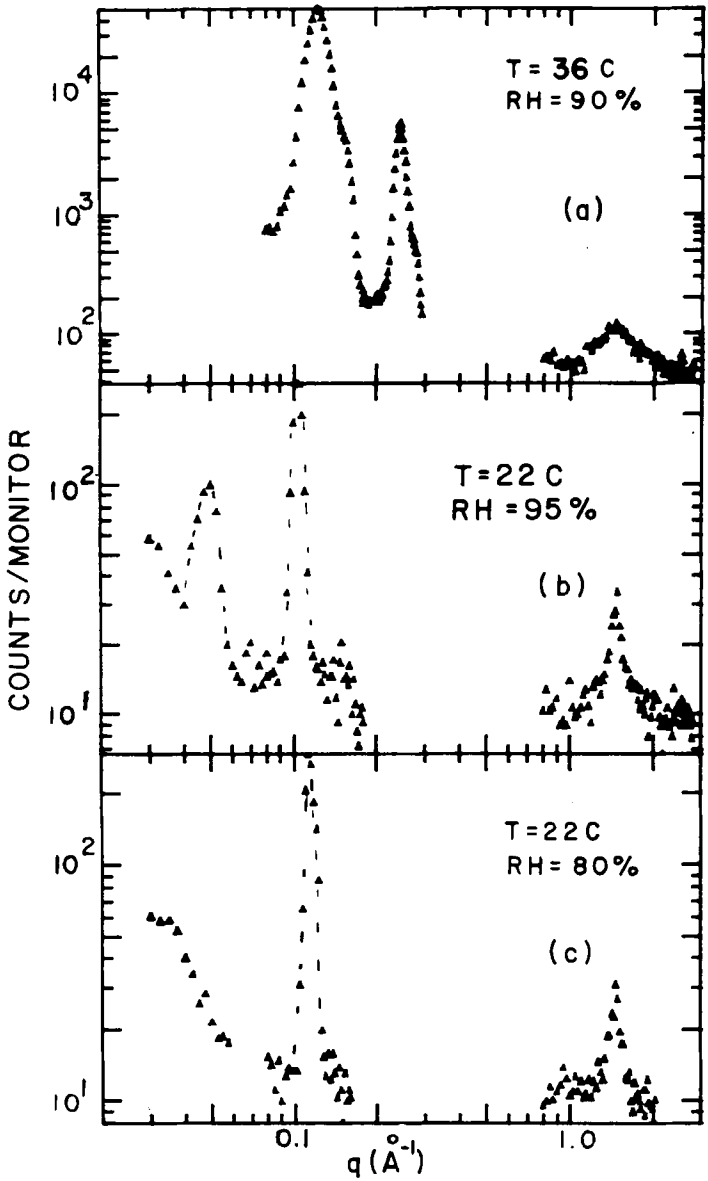

FIGURE 7 Longitudinal scans in reciprocal space plotted on a log-log scale of thick partially aligned films of DMPC (a)$L\alpha$, (b)$P_{\beta'}$ and (c)$L_{\beta'}$ phases. The dashed lines are added as a guide to the eye. Note the sharpening of the higher q ($\sim$1.4 Å^{-1}) peak indicative of long range intermolecular positional ordering in the layers in the $P_{\beta'}$ and $L_{\beta'}$ phases.

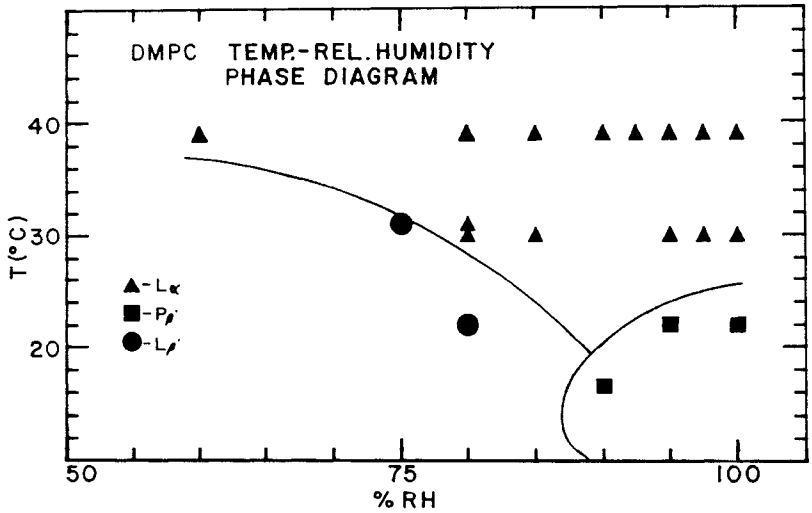

FIGURE 8 The temperature-relative humidity (or chemical potential) phase diagram for the DMPC-water binary system.

a vapor phase agree on a maximum value of adsorption for the water around 30% instead of the 40% obtained with bulk water. These results lead to a question concerning the position of the equilibrium phase boundary. We believe that the equilibrium state is obtained through equilibration of the mixture with the vapor rather than in the presence of excess water. On the basis of the experiments described above, we conclude that between 30% and 40% water concentration exists a region where the lamellar phase is metastable. We believe that this metastable phase is associated with the formation of vescicles.

Measurement of the interaction force between lamellae

Since we have the value of the chemical potential as a function of both the d-spacing and the concentration, we can apply the method used by Parsegian *et al.*[4] to measure the interaction force between lamellae. For a given vapor pressure P and temperature T, we have measured the d-spacing of a thick lipid-water film. Using the data from the T-C phase diagram, we can calculate the water concentration corresponding to this d-spacing. The thickness of the water layer is simply given by $d_w = C \cdot d$ since the densities of the lipids and the water are nearly equal.[13] The chemical potential μ is calculated using Eq.(1) and by dividing $\Delta\mu$ by the molar volume of water, we obtain

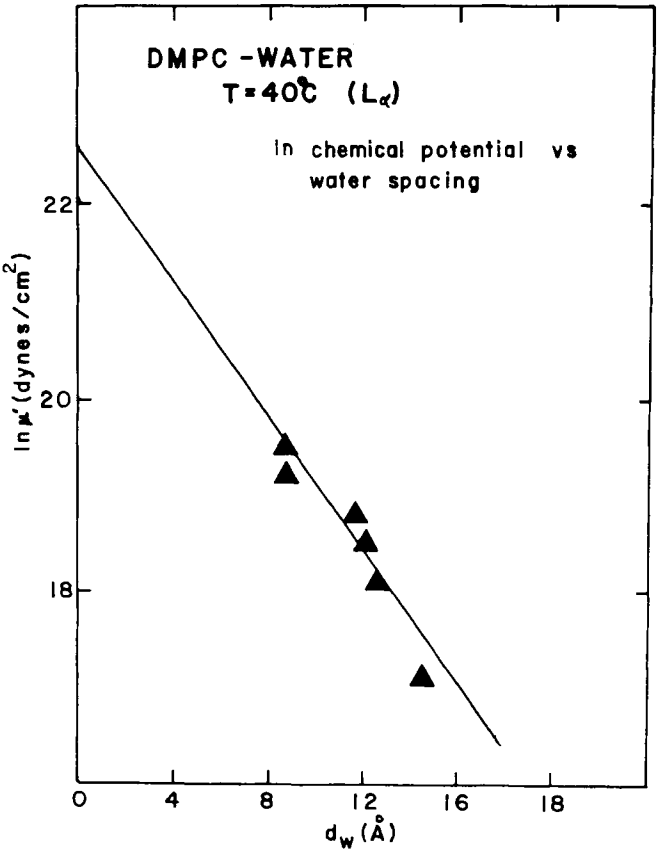

FIGURE 9 The log of the chemical potential versus the water layer thickness. The value of μ has been divided by the molar volume of water to obtain μ' in units of pressure.[4]

$\Delta\mu'$, the energy per unit volume. Figure 9 shows a semi-log plot of the value of the chemical potential $\Delta\mu'$ versus the separation distance d_w. We see that the data may be fitted to a straight line. This then suggests the existence of an exponential repulsive free energy of interaction, $\Delta\mu' = \Delta\mu_0' \exp(-d_w/\lambda)$. Fits of this equation to the weighted data yield values of $\lambda = 3.4 \pm 2.0$ Å and $\Delta\mu_0' = 3.8 \pm 2.5 \times 10^9$ dynes/cm^2. (Since the molar free energy is equal to the chemical potential, Figure 9 can also be interpreted as a plot of the free energy of interaction as a function of the intermembrane separation, d_w.) Such a functional form is usually attributed to the hydration interaction force.[3,4]

IV. REFLECTIVITY MEASUREMENTS

With the addition of the long, narrow, film holder (Figure 3), we can perform x-ray measurements in the reflection geometry. This allows us to measure the scattering along the plane-normal, z-direction. From the peak positions, we can determine the interplanar spacing, d. In addition to measuring the d-spacings, we can also gain information regarding the interplanar forces from the lineshapes. It was shown by Landau[14] and Peierls[15] that the mean square displacement of a plane about its equilibrium position for a one dimensional density modulation in a three dimensional medium diverges logarithmically with sample size. In this case, the x-ray structure factor is no longer described by the familiar Bragg scattering delta function. Instead the scattering is described by an algebraically decaying function which has the asymptotic form[18]:

$$S(0,0,q_z) \sim |(q_z - q_m)|^{-2+\eta_m} \qquad , q_\perp = 0 \tag{2a}$$

$$S(q_\perp,0,q_z) \sim |q_\perp|^{-4+2\eta_m} \qquad , q_z = q_m \tag{2b}$$

$$\eta_m = q_m^2 k_B T / 8\pi (BK)^{1/2} \tag{2c}$$

where q_z is along the plane normal direction, $q_\perp$ is parallel to the planes, $q_m = m2\pi/d$, $m = 1,2,3. .$ the order of the harmonic, K is the splay elastic modulus and B is the compression elastic modulus. Small values of η_1 have been measured in the smectic A phase of a thermotropic liquid crystal system using a high resolution x-ray scattering spectrometer.[17] Recently, large values of η_1 have been observed for a four component system of SDS, water, pentanol, and dodecane.[6]

Our reflectivity technique is well suited for the measurement of η_m. Since we are dealing with oriented single crystals, there is no need to powder average the data. Also, the reflected intensity from the films is quite strong. This allows us to collect good statistical data over short periods of time which lessens the chances of radiation damage to the sample. In addition, because we have access to a large portion of reciprocal space, we can perform scans along both the $(0,0,q_z)$ direction and the $(q_\perp,0,q_m)$ direction.

Using the VHR spectrometer on beamline X10A, we performed the longitudinal $(0,0,q_z)$ and transverse $(q_\perp,0,q_m)$ scans mentioned above. Figure 10 shows a typical set of scans about the sixth harmonic.

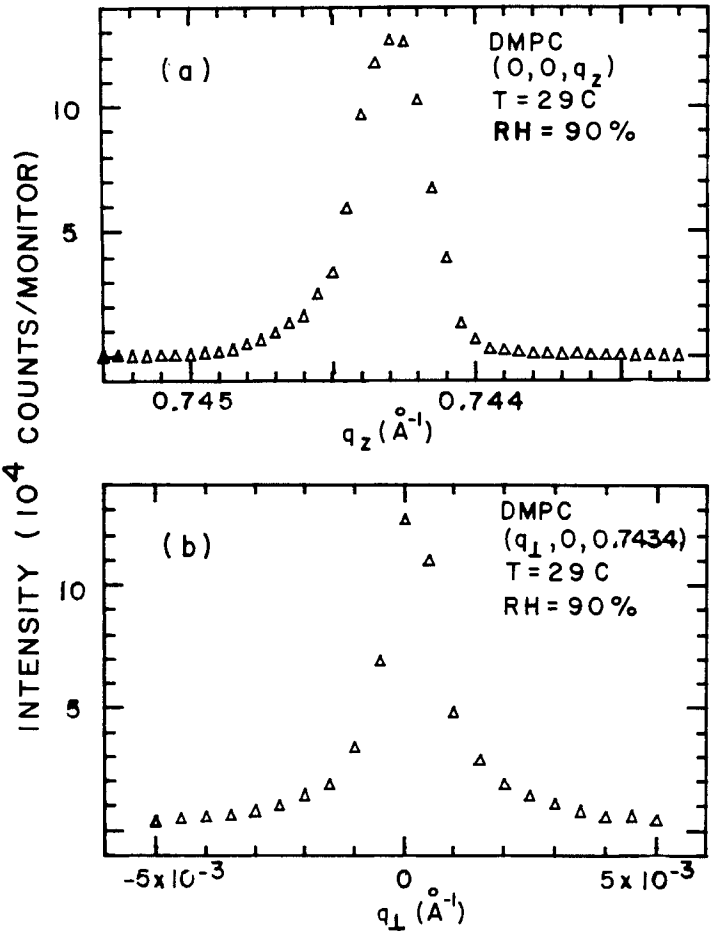

FIGURE 10 A longitudinal $(0,0,q_z)$ and a transverse $(q_\perp,0,q_z)$ scan through the sixth order harmonic of the interplanar peak.

From this figure, we see that the width of the transverse scan is approximately .09 degrees which indicates good mosaic alignment. With this same film, we performed sets of scans through the eighth harmonic. These $(0,0,q_z)$ scans are shown in Figure 11. The fact that we are able to measure the scattering through the eighth harmonic immediately suggests that thermal fluctuations are relatively; therefore, η_1 must be small. From Eq. (2c), we see that η_m will have its largest value for the highest harmonic. Figure 12 shows the eighth harmonic plotted along with the sixth harmonic and the resolution function. It is clear from this figure that the peak widths are larger

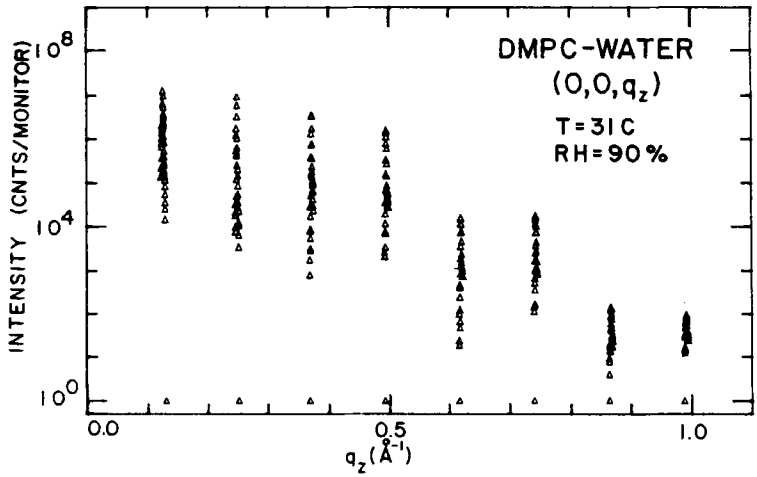

FIGURE 11 The first through the eigth order harmonic of the interplanar peak.

than the width of the resolution function. The intrinsic width of the peaks near $q_z = q_m$ is due to finite size effects.[6] This means that the power law behavior Eq. (2) can only be observed in the tails of the peaks. The region of the scattering away from the peak is shown plotted on a log-log scale in Figure 13. The slope of the resolution function falls off as $\sim q^{-3.4}$. Theoretically, one expects a fall off of

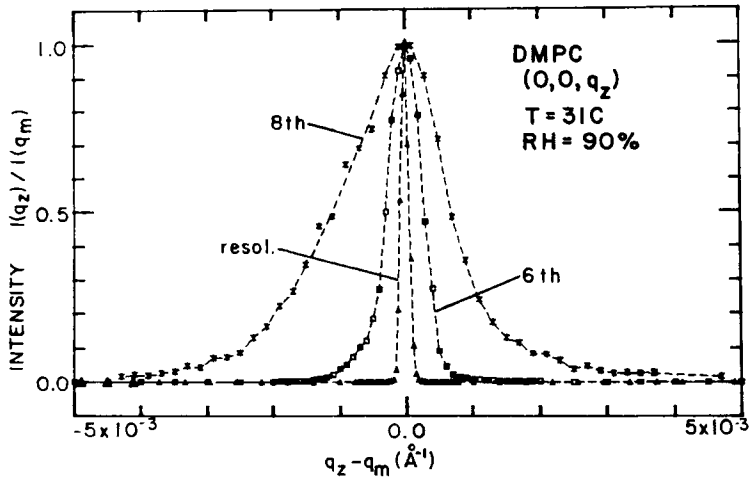

FIGURE 12 The sixth and the eighth order harmonics compared with the measured resolution function. The main contribution to the broadening of the peaks is the finite size effect.

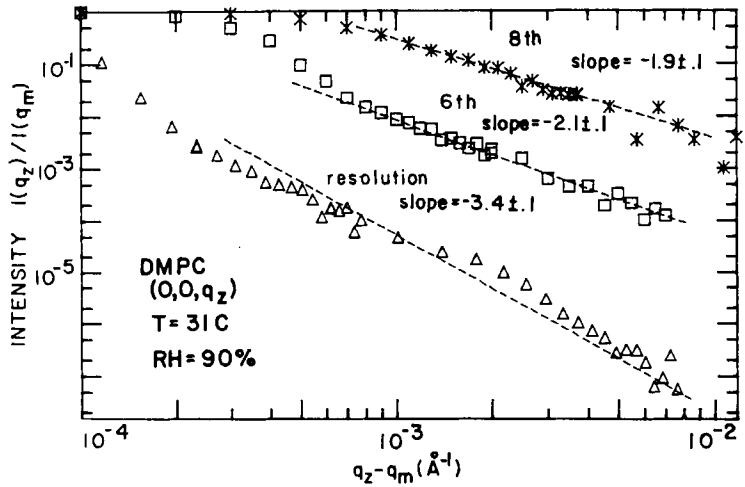

FIGURE 13 The tails of the sixth and eighth order harmonics compared with the tail of the resolution function. See text for discussion.

$q^{-4.0}$ (this is the expected value for the convolution of the scattering function of a double bounce Si(111) monochromator with the scattering function of a triple bounce Si(111) analyzer.[17] It is crucial that the magnitude of the slope of this resolution function be greater than 2.0 (see Eq. (2)) in order to unambiguously determine a value for the slope of the scattering from the sample. The sixth harmonic has a slope of -2.1 ± 0.1 (Figure 13) but because of the uncertainty in this slope we cannot determine a value for η_6. The eighth harmonic is the first data for which the magnitude of the slope (including the uncertainty) is less than 2.0. If we assume that η_8 is just under the measurable value of 0.10,[6] then we can estimate an upper bound on η_1 of $(0.10/64) = 0.0016$.

To see whether this small value of η_1 can be understood, we compare this value with an estimate of η_1 from our interplanar force measurements discussed in the previous section. We note that the reflectivity measurements are carried out at a fixed water chemical potential. In this case the molar free energy, g, is simply equal to the chemical potential. The bulk compressibility, B, is given in terms of the chemical potential per unit volume, $\Delta\mu'$, as

$$B = d^2(\partial^2 \Delta\mu'/\partial d_w^2) \tag{3}$$

and in the hydration force model $\Delta\mu' = \Delta\mu_0' \exp(-d_w/\lambda)$ therefore,

$$B = \Delta\mu_0'(d^2/\lambda^2) \exp(-d_w/\lambda). \tag{4}$$

If we use d and d_w corresponding to the largest water spacing and the values obtained for λ and $\Delta\mu_0'$ from our fit (section III), we find that $B = 1.6 \pm .9 \times 10^{10}$ dynes/cm^2. If we combine this with the measured value of $K_c = Kd \sim 1.5 \times 10^{-12}$ ergs,[18] Eq. 2c yields $\eta_1 = 1.3 \pm 0.4 \times 10^{-3}$. This value is consistent with our limiting value of η_1 obtained directly from reflectivity measurements of the structure factor. The small value of η_1 thus can be attributed to the short range intermembrane interaction forces.

V. CONCLUSIONS

We have presented a new technique for growing oriented, large domain, films of DMPC-water mixtures. This is accomplished using a humidity controlled oven with which we can vary both the temperature and the chemical potential of the sample. With this apparatus, we have demonstrated the feasibility of x-ray scattering studies of lipid-water films. In particular, we have measured the (T-μ) and (T-C) phase diagrams for this system. A comparison of these two diagrams suggests the existence of a metastable state in the bulk samples for $30\% \leq C \leq 40\%$. Also, we have utilized this data in a study of the interplanar forces, and we find that as a function of water layer thickness, d_w, these forces behave exponentially. This suggests that the source of the repulsive interplanar interaction is the hydration force.

By using a new film holder design, we have expanded the freely suspended film technique to include reflectivity measurements. This allows us to measure the x-ray scattering amplitude along both the in-plane and out-of-plane directions. With this reflectivity data, we estimate an upper limit to the Landau-Peierls constant $\eta_1 = 0.0016$ which describes the algebraic decay of layer correlations. We have also calculated a value of $\eta_1 = 0.001$ from our interplanar force measurements which is in agreement with our estimated limit. This small value of η_1 shows that thermal fluctuations are weak in this system.

In the future, much new information about lipid-water systems may be learned using the freely suspended film technique. Since oriented films are grown, the precise structures of the $L_{\beta'}$ and the $P_{\beta'}$ phases may be determined. This includes the possibility of measuring both the wave vector and the polarization vector of the long wavelength modulation in the $P_{\beta'}$ phase. Also, with the oriented samples, the inter- as well as the intra-layer correlations may be established. For example, we have preliminary data on the $L_{\beta'}$ phase which indicates that the interlayer positional correlations between the in-plane dis-

torted triangular lattices can be extremely short range across the water layers separating the membranes. Ultimately, this technique may be used to study single lipid bilayers as models of cell membranes.

Acknowledgments

This research was supported in part by a joint Industry/University Grant, No. DMR-8307157. We would like to acknowledge the helpful assistance of the Exxon staff members at the Exxon beamline at the National Synchrotron Light Source, Brookhaven National Laboratory (supported by DOE). We gratefully acknowledge discussions with B. Ocko and P. S. Pershan. We would also like to thank K. D'Amico and E. Sirota for their assistance at the beamline. Finally we would like to thank W. Varady, P. Bataille, and D. Chu for their assistance in the preparation of this manuscript.

References

1. V. Luzzati, *Biol. Membr.*, **1**, 71(1968); V. Luzzati, T. Gulik-Krzywicki and A. Tardieu, Nature, **218**, 1031 (1968).
2. P. R. Cullis and M. J. Hope, in *Biochemistry of Lipids and Membranes* (D. E. Vance and J. E. Vance, eds.), Benjamin/Cummings, Menlo Park (1985).
3. J. N. Israelachvili, "Intermolecular and Surface Forces," Acedemic Press, Orlando (1985).
4. V. A. Parsegian, N. Fuller and R. P. Rand, *Proc. Natl. Acad. Sci.*, **76**, 2750 (1979); D. M. LeNeveu, R. P. Rand, V. A. Parsegian and D. Gingell, *Biophys. J.*, **18**, 209 (1977).
5. W. Helfrich, Z. Naturforsch., **33a**, 305 (1978).
6. C. R. Safinya, D. Roux, G. S. Smith, S. K. Sinha, P. Dimon, N. A. Clark and A. M. Bellocq, *Steric Interactions in a Model Membrane System: A Synchrotron X-Ray Study*, Phys. Rev. Lett. (Nov. 4), 1986.
7. M. J. Janiak, D. M. Small and G. G. Shipley, *J. Biol. Chem.*, **254**, 6068 (1979).
8. C. Y. Young, R. Pindak, N. A. Clark and R. B. Meyer, *Phys. Rev. Lett.*, **40**, 773 (1978).
9. D. E. Moncton and R. Pindak, *Phys. Rev. Lett.*, **43**, 701 (1979).
10. J. Collett, L. B. Sorenson, P. S. Pershan, R. J. Birgeneau, J. D. Litster and J. Als-Nielsen, *Phys. Rev. Lett.*, **49**, 553 (1982); J. Collett, L. B. Sorenson, P. S. Pershan, and J. Als-Nielsen, Phys. Rev. A, **32**, 1036 (1985).
11. S. M. Gruner, *Rev. Sci. Instrum.*, **52**, 134 (1981).
12. L. Powers and P. S. Pershan, *Biophys. J.*, **20**, 137 (1977).
13. A. Tardieu, V. Luzzati and F. C. Reman, *J. Mol. Biol.*, **75**, 711 (1973).
14. L. D. Landau, in Collected Papers of L. D. Landau (ed by D. Terr Haar), Gordon and Breach, New York (1965) p. 209.
15. R. E. Peierels, *Helv. Phys. Acta*, **7**, 81 (1974).
16. A. Caillé, *C.R. Acad. Sci.*, **274B**, 891 (1972).
17. J. Als-Nielsen, R. J. Birgeneau, M. Kaplan, J. D. Litster and C. R. Safinya, *Phys. Rev. Lett.*, **39**, 1668 (1977).
18. M. B. Schneider, J. T. Jenkins and W. W. Webb, *Biophys. J.*, **45**, 891 (1984).
19. S. G. J. Mochrie, A. R. Kortan, R. J. Birgeneau and P. M. Horn, *Z. Phys. B.*, **62**, 79 (1985).
20. J. Als-Nielsen, F. Christensen and P. S. Pershan, *Phys. Rev. Lett.*, **48**, 1107 (1982).
21. P. S. Pershan, Phys. Today, **35**, 34 (1982).